Journal of *Marine Science and Engineering*

MDPI

Article

Numerical Performance Model for Tensioned Mooring Tidal Turbine Operating in Combined Wave-Current Sea States

Song Fu * and Cameron Johnstone

Energy Systems Research Unit, Department of Mechanical and Aerospace Engineering, University of Strathclyde, Glasgow G1 1XQ, UK; cameron.johnstone@strath.ac.uk
* Correspondence: song.fu@strath.ac.uk

Abstract: This study proposes the design of a tidal turbine station keeping system based on the adoption of a tensioned mooring system. Damping is introduced to investigate its effect on the reduction in the peak load experienced by tidal turbines during their operational lives in high-energy wave–current environments. A neutrally buoyant turbine is supported using a tensioned cable-based mooring system, where tension is introduced using a buoy fully submersed in water. The loads on the turbine rotor blades and buoy are calculated using a wave and current-coupled model. A modelling algorithm is proposed based on inverted pendulums, which respond to various sea state conditions, to study the behaviour of the system as well as the loads on blades. The results indicate that the tensioned mooring system reduces the peak thrust on the turbine and validates the applicability of the model.

Keywords: tidal turbine; modelling; mooring system; blade loading; wave–current interaction

Citation: Fu, S.; Johnstone, C. Numerical Performance Model for Tensioned Mooring Tidal Turbine Operating in Combined Wave-Current Sea States. *J. Mar. Sci. Eng.* **2021**, *9*, 1309. https://doi.org/10.3390/jmse9111309

Academic Editor: Eugen Rusu

Received: 14 September 2021
Accepted: 15 November 2021
Published: 22 November 2021

1. Introduction

Tidal-stream energy can contribute significantly to global renewable energy generation, and the UK has an estimated 10–15% of the global harvestable tidal resources [1]. Tidal stream turbine (TST) technology has developed to a stage where first large-scale commercial facilities are being deployed. For example, the MeyGen project, which has exported 17 GWh to the grid as of June 2019 [2], is proving to be a reliable and economically viable renewable energy source. However, the durability of such projects is a complicated subject because the loads on TSTs vary widely owing to the unsteady marine environment. Therefore, it is challenging to achieve 10–25 year fatigue lives for turbine. There are six main types of tidal energy convertors (TEC), namely, horizontal axis turbine, vertical axis turbine, oscillating hydrofoil, enclosed tips (venturi), archimedes screw, and tidal kite [3].

The design of tidal turbine station keeping systems varies based on the turbine architecture being considered and the method of attachment to the seabed being employed. At present, gravity-based structures, drilled monopiles, and drilled pin pile tripods are three widely used support structures for tidal turbines. To make tidal current generation commercially competitive with the traditional types of energy, the industry must focus on reducing the cost of generation of the tidal-stream energy. Two main cost factors that must be targeted are the installation and maintenance of the equipment. Therefore, flexible mooring-based systems are being used for the station keeping of floating tidal turbines, such as CoRMaT [4] and Minesto 'Tidal Kite'.

Modelling methods to investigate the dynamics of a tensioned mooring-based turbine have been discussed in this paper. The analysis and control of the marine mooring and cable system are presented in [5], where the method is used to solve the dynamics of the ship and offshore platform mooring system. Mooring systems from the offshore oil and gas and ship industry have been developed and applied to design some wave energy converters [6,7]. Research shows that the single point mooring system is suggested to be applied in large dimension wave energy converters owing to the ability to minimise

environmental loads [8]. However these approaches are applied generally to mooring lines that are not fully tensioned and connected to a floating structure on the surface of water.

A submerged floating tidal current hydrokinetic turbine system named GEMSTAR was presented by [9]. GEMSTAR is a project developed at the the University of Naples and the first prototype has been tested in the towing tank. It reports that problems may arise in the design of the mooring system and structural optimization, as a consequence of the high loads due to turbine thrust and required buoyancy. However, the methods to calculate the thrust, torque, the buoyancy and other dynamic characteristics of the tensioned mooring turbine have not been investigated so far. The objective of this research is to build up a numerical model to simulate these characteristics of the tensioned mooring turbine.

In this paper, the system is assumed to be an inelastic mooring, and it is modelled based on an inverted pendulum system. A coupled pendulum with an external drive is expected to experience complicated dynamics. The existence of irregular vibrations and both periodic and chaotic trajectories of a mathematical double pendulum system is proven in [10]. The stabilisation of the inverted pendulum, which is a highly nonlinear system, has been studied extensively for control education and research purposes. However, the moored turbine system is a quasi-dynamic system owing to the external forces. The external forces such as loading on the turbine rotor blades and buoy are calculated using a wave coupled blade element momentum theory (BEMT). The code was developed at the University of Strathclyde to analyse the loading occurring on a turbine rotor-drive train when operating in energetic wave–current flow conditions [11].

2. Methodology

The focus of this study is to present a methodology to assess the behaviour of a neutrally buoyant turbine supported from a tensioned cable-based mooring system, where tension is introduced using a buoy working as a damper and fully submersed in water. The schematic of the system in operation is depicted in Figure 1.

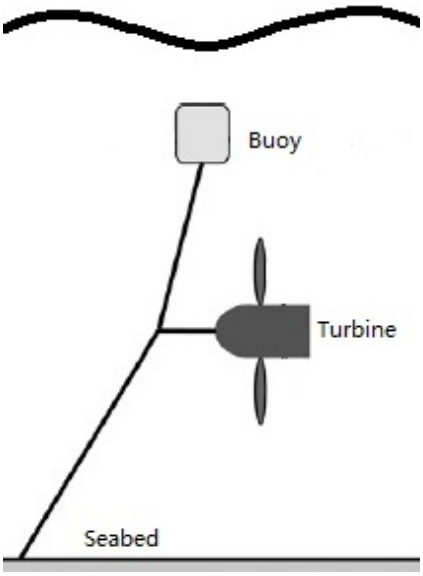

Figure 1. Schematic of tensioned mooring turbine in operation.

In order to solve the dynamics of the tensioned mooring turbine in a wave–current coupled environment efficiently. The tensioned mooring system is modelled as a special type of triple pendulum, called an inverted flail. It consists of three pendulums: the first one is attached to a fixed point considered to be an anchor and to its end mass; the other two pendulums are joined. An original flail system without the external drive and gravity field is depicted in Figure 2. This system was analysed in [12].

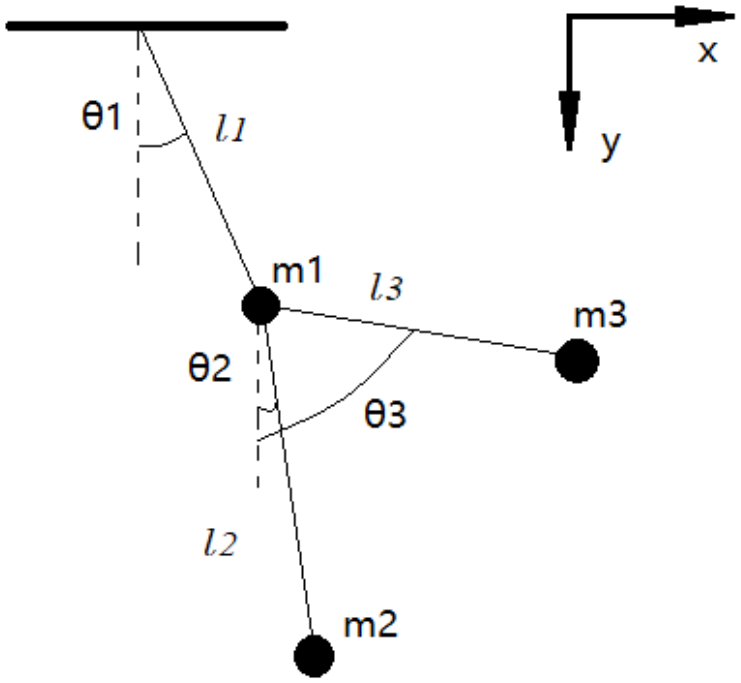

Figure 2. Geometry of flail pendulum.

Unlike the original flail system, the tensioned mooring supported turbine is driven by external forces as the loads on the turbine and buoy. A wave–current coupled BEMT was utilised to calculate the loads on the turbine rotor blades. The code was developed at the University of Strathclyde to analyse the loading on a turbine rotor-drive train when operating in energetic wave–current flow conditions [13]. In addition, owing to the turbine being able to move and respond to the moving flow field generated by the waves, the resulting motions due to flow field interactions must be taken into consideration. By coupling the tensioned mooring system with the forces obtained from BEMT as the external drive forces in wave–current environments, it is efficient to calculate the dynamics of the turbine and mooring lines together at each time step in a long simulation window.

2.1. Model of Mooring Supported Turbine

The mooring lines are assumed to continuously be in tension during operation. Therefore, this system can be modelled as an inverted flail pendulum in order to calculate its dynamics; Figure 3 provides the model for the three elements in flail pendulum. Equations of motion of the pendulum system can be derived using the following Lagrange's equation:

$$\frac{d}{dt}\left(\frac{\partial L}{\partial \dot{\theta}_i}\right) - \frac{\partial L}{\partial \theta_i} = Q_i, \tag{1}$$

where L = T − V is defined as the Lagrangian of the system, T is the kinetic energy and V the potential energy of system.

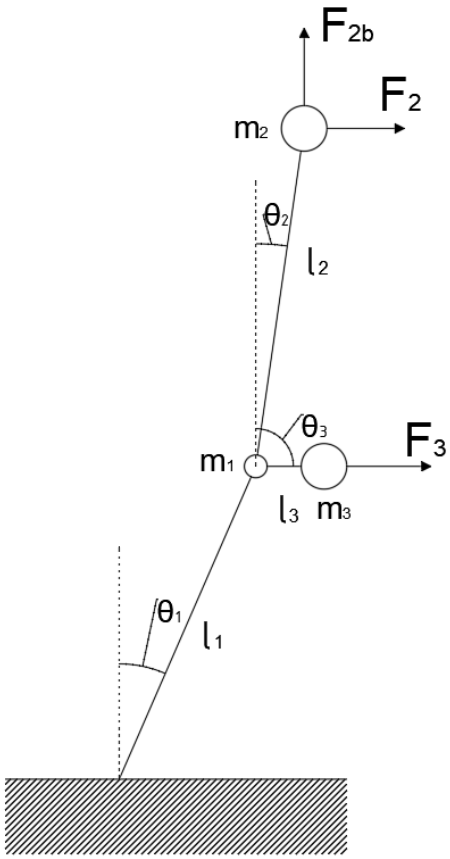

Figure 3. Multi-pendulum system with a finite number of rods and masses.

When an external force function Q_i is not considered, then the point of anchor is chosen, which is suspension of the first pendulum as the origin, and angles are measured from the vertical line; as shown in Figure 3, the Lagrangian of the system can be written as:

$$\begin{aligned} L = \frac{1}{2}(m_1 + m_2 + m_3)l_1^2\dot{\theta}_1^2 + \frac{1}{2}m_2 l_2^2\dot{\theta}_2^2 + \frac{1}{2}m_3 l_3^2\dot{\theta}_3^2 \\ + m_2 l_1 l_2 \dot{\theta}_1\dot{\theta}_2 \cos(\theta_1 - \theta_2) + m_3 l_1 l_3 \dot{\theta}_1\dot{\theta}_3 \cos(\theta_1 - \theta_3) \\ + (m_1 + m_2 + m_3) g l_1 \cos\theta_1 + m_2 g l_2 \cos\theta_2 + m_3 g l_3 \cos\theta_3, \end{aligned} \tag{2}$$

where m_1 is the lumped mass of three mooring lines at the connection node, m_2 represents the mass of buoy, m_3 represents the mass of the turbine. l_1, l_2 and l_3 are the length of each segment. θ_1, θ_2 and θ_3 are generalised coordinates as shown in Figure 3.

It is assumed that the turbine and the buoy are neutrally buoyant, so the potential energy terms in Equation (2) can be eliminated. The new Lagrangian of the system becomes:

$$\begin{aligned} L = \frac{1}{2}(m_1 + m_2 + m_3)l_1^2\dot{\theta}_1^2 + \frac{1}{2}m_2 l_2^2\dot{\theta}_2^2 \\ + m_2 l_1 l_2 \dot{\theta}_1\dot{\theta}_2 \cos(\theta_1 - \theta_2) \\ + \frac{1}{2}m_3 l_3^2\dot{\theta}_3^2 + m_3 l_1 l_3 \dot{\theta}_1\dot{\theta}_3 \cos(\theta_1 - \theta_3). \end{aligned} \tag{3}$$

Substituting Equation (3) into Equation (1) yields the Euler–Lagrange differential equations of the system:

$$\begin{aligned} (m_1 + m_2 + m_3)l_1^2\ddot{\theta}_1 + m_2 l_1 l_2 \ddot{\theta}_2 \cos(\theta_1 - \theta_2) \\ - m_2 l_1 l_2 \dot{\theta}_2^2 \sin(\theta_1 - \theta_2) + m_3 l_1 l_3 \ddot{\theta}_3 \cos(\theta_1 - \theta_3) \\ - m_3 l_1 l_3 \dot{\theta}_3^2 \sin(\theta_1 - \theta_3) = Q_1 \end{aligned} \tag{4}$$

$$m_2 l_2^2 \ddot{\theta}_2 + m_2 l_1 l_2 \ddot{\theta}_1 \cos(\theta_1 - \theta_2) - m_2 l_1 l_2 \dot{\theta}_1^2 \sin(\theta_1 - \theta_2) = Q_2 \quad (5)$$

$$m_3 l_3^2 \ddot{\theta}_3 + m_3 l_1 l_3 \ddot{\theta}_1 \cos(\theta_1 - \theta_3) - m_3 l_1 l_3 \dot{\theta}_1^2 \sin(\theta_1 - \theta_3) = Q_3, \quad (6)$$

where Q_1, Q_2 and Q_3 are now generalised moments with respect to θ_1, θ_2 and θ_3. In this case, Q_3 equates to the momentum thrust develop by a turbine loading, where this is operating under combined wave and currents conditions. Q_2 relates to the buoyant forces occurring on the floater, which are considered in the form of buoyancy and wave excitation forces. Q_1 will be obtained from the relationship between Q_2 and Q_3. According to Anli and Ohlhoff [14,15], the generalised force can be obtained as:

$$Q_k = \sum_{i=1}^{n} F_i \frac{\partial r_i}{\partial q_k}, \quad (7)$$

where Q_k is the Generalised force associated with the *kth* Euler-Lagrange differential equation, F_i is the external force, r_i is the position of the point of application and q_k is the generalised coordinate.

Thus, substituting Equation (7) to the generalised coordinates with respect to θ_1, θ_2 and θ_3, the generalised moments for this system are given as:

$$Q_1 = F_3 l_1 \cos\theta_1 - F_{2b} l_1 \sin\theta_1 + F_2 l_1 \cos\theta_1 \quad (8)$$

$$Q_2 = F_2 l_2 \cos\theta_2 - F_{2b} l_2 \sin\theta_2 \quad (9)$$

$$Q_3 = F_3 l_3 \cos\theta_3. \quad (10)$$

When the generalized moments are obtained, the Euler–Lagrange differential equations of the system can be solved with given initial conditions. Substituting Equations (8)–(10) into Equations (4)–(6) then dividing by l_1, l_2 and l_3 yields:

$$(m_1 + m_2 + m_3) l_1 \ddot{\theta}_1 + m_2 l_2 \ddot{\theta}_2 \cos(\theta_1 - \theta_2) - m_2 l_2 \dot{\theta}_2^2 \sin(\theta_1 - \theta_2) + m_3 l_3 \ddot{\theta}_3 \cos(\theta_1 - \theta_3) - m_3 l_3 \dot{\theta}_3^2 \sin(\theta_1 - \theta_3) = F_3 \cos\theta_1 - F_{2b} \sin\theta_1 + F_2 \cos\theta_1 \quad (11)$$

$$m_2 l_2 \ddot{\theta}_2 + m_2 l_1 \ddot{\theta}_1 \cos(\theta_1 - \theta_2) - m_2 l_1 \dot{\theta}_1^2 \sin(\theta_1 - \theta_2) = F_2 \cos\theta_2 - F_{2b} \sin\theta_2 \quad (12)$$

$$m_3 l_3 \ddot{\theta}_3 + m_3 l_1 \ddot{\theta}_1 \cos(\theta_1 - \theta_3) - m_3 l_1 \dot{\theta}_1^2 \sin(\theta_1 - \theta_3) = F_3 \cos\theta_3. \quad (13)$$

The external forces on the buoy and turbine are depicted in Figure 4. In this paper, the wave excitation forces on the turbine are assumed to be ignored.

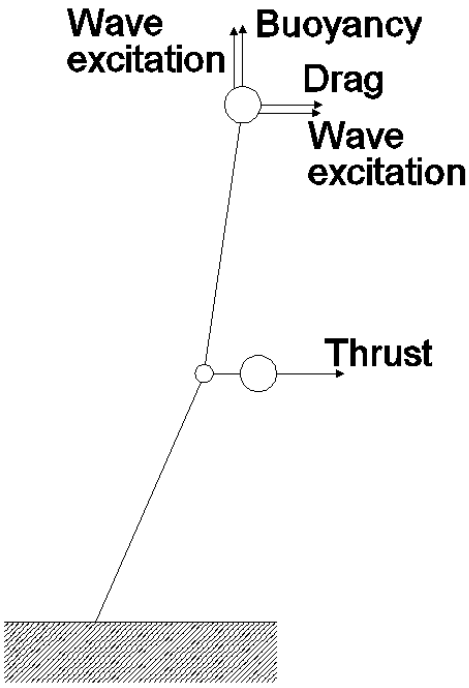

Figure 4. Forces on the system.

Wave excitation is considered to be a factor of the system. The buoy will be excited by the wave at a different magnitude based on its shape. The wave excitation in two directions can be defined as the exciting force and drift force, based Wu [16]. The thrust on the turbine can be obtained using an ESRU in-house BEMT code [11]. Modifications have been made in the original code owing to the relative velocity between the turbine and inflows:

$$\mathbf{U} = \mathbf{u} - \mathbf{U}_{\mathrm{T}}, \tag{14}$$

where $\mathbf{u}$ is the inflow velocity, which is calculated using the wave–current interaction model; $\mathbf{U}_{\mathrm{T}}$ is the inertia velocity of the turbine, which is the velocity generated by the motions of turbine in waves. It can be calculated in vertical and horizontal directions as:

$$\mathbf{U}_{\mathrm{T}} = \frac{\partial}{\partial \Delta t}(\mathbf{X}^{\mathrm{it}}_{\mathrm{turbine}} - \mathbf{X}^{\mathrm{it}-1}_{\mathrm{turbine}}), \tag{15}$$

where it is time step count number, $\mathbf{X}_{\mathrm{turbine}}$ is the turbine position and Δt is the time difference. The buoy is assumed to be spherical. The drag force is also calculated from the BEMT code. The relative velocity between the buoy and inflows must be considered:

$$\mathbf{V} = \mathbf{u} - \mathbf{U}_{\mathrm{B}}. \tag{16}$$

$\mathbf{u}$ can be calculated using the wave–current model based on the coordinates of the buoy. $\mathbf{U_B}$ is the inertia velocity of the buoy:

$$\mathbf{U}_{\mathrm{B}} = \frac{\partial}{\partial \Delta t}(\mathbf{X}^{\mathrm{it}}_{\mathrm{buoy}} - \mathbf{X}^{\mathrm{it}-1}_{\mathrm{buoy}}). \tag{17}$$

2.2. Flow Diagram

The original in-house BEMT code for wave–current environments is based on a rigid supported turbine, where the position of the turbine does not change with time. However, the coordinates of the mooring supported turbine are variable with time and the relative velocity must be calculated using the relative motion between the turbine and wave–current inflow. Figure 5 depicts the main process of the simulation. The process nodes with the dark background are works based on this study, which are different from the original BEMT.

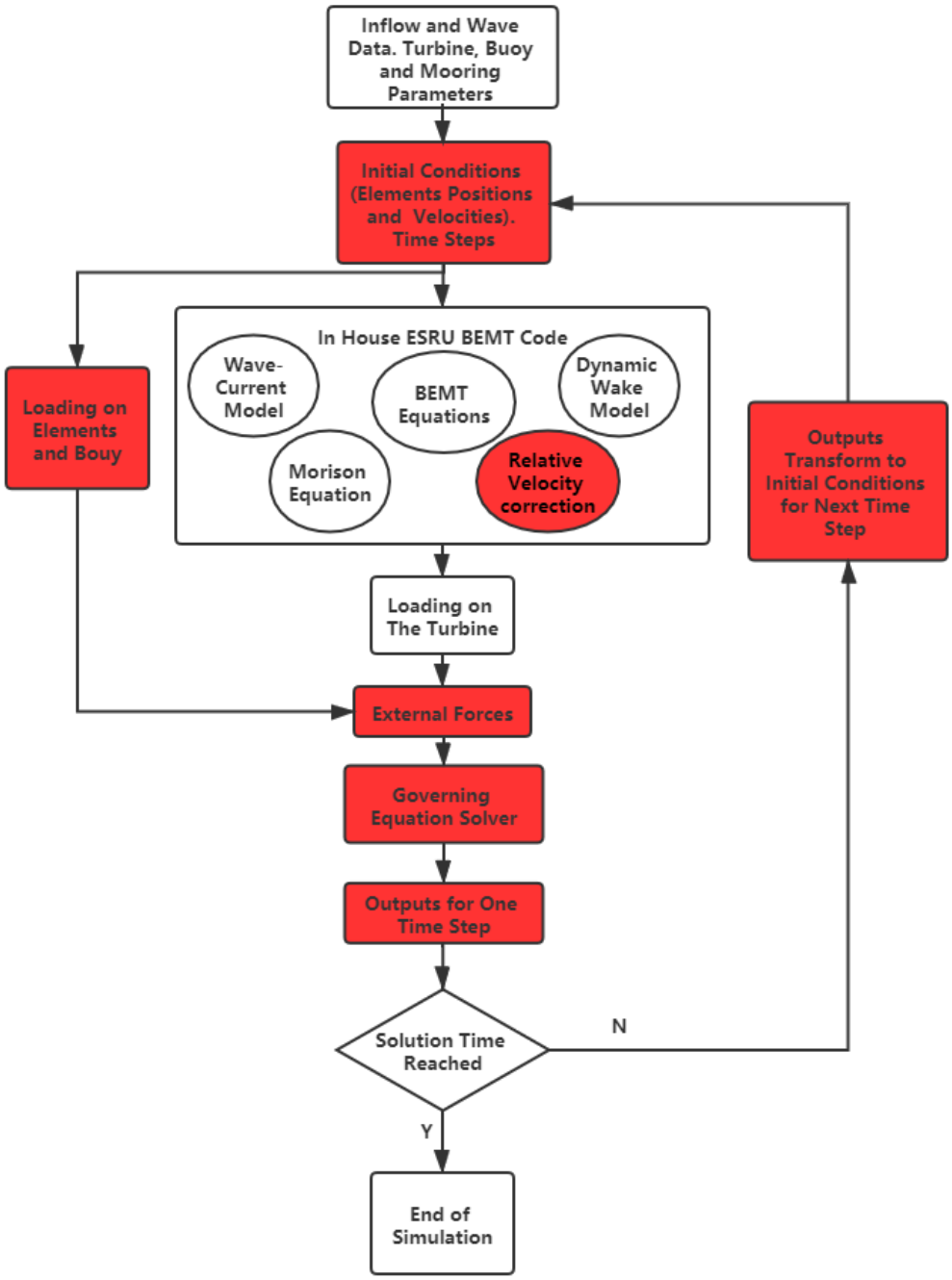

Figure 5. Solution process.

There are some variable input parameters that can be defined by users for different mooring turbine devices. The state of motion for the system in the first time step is defined by the initial conditions. The loads on each mooring element and buoy are obtained as the external forces, whereas the load on the turbine is calculated using the BEMT code while modifying the relative velocity. After the external forces are determined, the governing equation for the "flail" system with a finite number of segments can be solved by an ordinary differential equations solver to obtain the new state of motion of the system. The new values are used as the initial conditions for the next time step until the simulation culminates.

For the wave–current model module, calculations of the horizontal and vertical particle velocities are related to the horizontal and vertical coordinates of the turbine in different wave theories. The coordinates of the turbine and buoy hinge nodes are x_{turbine}, y_{turbine},

x_{buoy} and y_{buoy}. Because the vertical particle velocities are varied along blades, the blade element coordinates are:

$$x_{\text{element}} = x_{\text{turbine}} + h_{\text{element}}\cos\phi \tag{18}$$

$$y_{\text{element}} = y_{\text{turbine}} + h_{\text{element}}\sin\phi, \tag{19}$$

where h_{element} is the element position on the blade and ϕ is the pitch angle of the turbine. Assume that the turbine is nearly horizontal during the operation and the pitch angle is 0 degree. The element coordinates become:

$$x_{\text{element}} = x_{\text{turbine}} \tag{20}$$

$$y_{\text{element}} = y_{\text{turbine}} + h_{\text{element}}. \tag{21}$$

Next, substitute these coordinates into wave models. Then, this module is modified to work for the mooring supported turbine.

The relative velocity modification of the inflow velocity must be considered in not only the BEMT equation but also the dynamic wake model and Morison equation.

Based on the methodology adopted, the dynamic inflow affects the BEMT model [17–19]. On a blade element bounded by radii R_1 and R_2 as shown in Figure 6, the momentum thrust equation depends on the time derivative of axial induction factor $\dot{a}$ as:

$$\mathrm{d}F_{\text{A}} = 2\mathbf{u}a\dot{m} + \mathbf{u}m_{\text{A}}\dot{a}, \tag{22}$$

where $\dot{m}$ is the mass flow through the intersecting fluid annulus, a is the axial induction factor, and m_{A} is the apparent mass of the blade section.

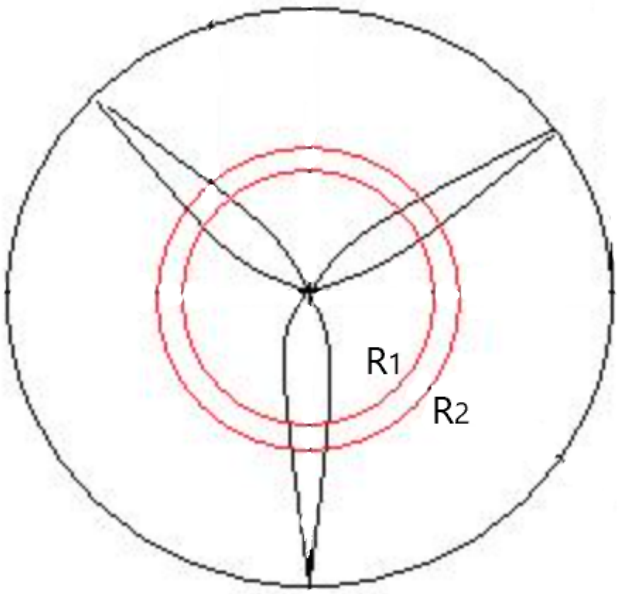

Figure 6. Blade element bounded by radii R_1 and R_2.

The mass flow through the annular element can be calculated as:

$$\dot{m} = \rho\mathbf{u}(1-a)\mathrm{d}A, \tag{23}$$

where ρ is the density of water and $\mathrm{d}A = \pi(R_2^2 - R_1^2)$.

For a turbine of radius R, Tuckerman [20] suggests that the apparent mass acting on the rotor can be approximated by an enclosing fluid ellipsoid, which can be expressed, through the use of potential flow theory, as:

$$m_{\mathrm{A}} = 8/3\rho R^3. \tag{24}$$

Substituting Equations (23) and (24) into Equation (22) and dividing each term by π, ρ, $\mathbf{u}$, and $\mathrm{d}A$ and multiplying by 2, then replacing the in flow velocity with the relative velocity U_x which is the horizontal component of relative velocity $\mathbf{U}$. The final form of the unsteady thrust coefficient for an annulus can be obtained as:

$$C_{\mathrm{FA}} = 4a(1-a) + \frac{16}{3\pi U_x}\frac{(R_2^3 - R_1^3)}{(R_2^2 - R_1^2)}\dot{a}. \tag{25}$$

Substituting thrust coefficient $C_{\mathrm{T}} = 4a(1-a)$ into Equation (25) gives:

$$C_{\mathrm{FA}} = C_{\mathrm{T}} + \frac{16}{3\pi U_x}\frac{(R_2^3 - R_1^3)}{(R_2^2 - R_1^2)}\dot{a}. \tag{26}$$

The last term on the right-hand side of Equation (26) can be used to calculate the additional force from the dynamic wake effects.

The inertial force caused by fluid acceleration, which is the added mass around a rotating blade section can be expressed as Morison equation, as presented by Buckland [21] and Chapman [22]. The inertial force per unit length, $\mathrm{d}l$ in the wave propagation direction on a submerged body can be calculated as:

$$\mathrm{d}F_{\mathrm{in}} = \rho C_{\mathrm{m}} A \frac{\partial \mathbf{u}}{\partial t}\mathrm{d}l, \tag{27}$$

where A is the cross horizontal sectional area parallel to the flow and C_{m} is the inertia coefficient, which is expressed as:

$$C_{\mathrm{M}} = 1 + C_{\mathrm{A}} = 1 + \frac{M_{\mathrm{A}}}{\rho A \mathrm{d}l'}, \tag{28}$$

where M_{A} is the added mass for a blade element.

For blade elements, the added mass in axial and tangential directions can be approximated with that of a fixed pitched plate as per Theodorsen's theory [23]:

$$M_{\mathrm{A,axial}} = \rho\pi(\frac{c\sin\beta}{2})^2\mathrm{d}l \tag{29}$$

$$M_{\mathrm{A,tan}} = \rho\pi(\frac{c\cos\beta}{2})^2\mathrm{d}l, \tag{30}$$

which are the masses of the enclosing fluid cylinders with radii r of half the vertical and horizontal chord components c of the respective blade sections with section angle β [24].

Substituting Equations (28)–(30) into Equation (27) and plugging the components of relative velocity $\mathbf{U}$ into the equation gives the equations for the inertia forces in the axial and tangential directions for a blade element as:

$$\mathrm{d}F_{\mathrm{in,axial}} = \rho(1 + \frac{\pi((c\sin\beta)/2)^2}{A_\alpha})A_\alpha\frac{\partial U_x}{\partial t}\mathrm{d}r \tag{31}$$

$$\mathrm{d}F_{\mathrm{in,tan}} = \rho(1 + \frac{\pi((c\cos\beta)/2)^2}{A_\alpha})A_\alpha\frac{\partial U_y}{\partial t}\mathrm{d}r, \tag{32}$$

where A_α is the cross-sectional area of the airfoil at the blade section.

When the external forces based on the initial conditions for the first time step are calculated using the BEMT equations with the wave–current model, dynamic wake model, and Morison equations, the system Lagrange equation solver begins to solve the differential equations of motion for the mooring supported turbine. Next, the new values and angular

velocities $\dot{\theta}_i$ for each segment are obtained to serve as the new initial conditions for the next time step. This loop continues until the time step reaches the end time of the simulation.

3. Initial Conditions and System Parameters

This study focuses primarily on external forces, which are buoyancy and wave–current-coupled forces. Sea states with regular and irregular waves were investigated. The wave data were collected by the UK Offshore Operators Association and were provided by British Oceanographic Data Center [25]. In this study, parameters of a 1 MW turbine and mooring system were applied to deep water. Parameters given below were fixed to control the number of variables. The material for the mooring line was chosen to be Dyneema, whose density is close to that of water. There were three sets of system parameters in each model, two of them were Dyneema mooring and one was steel mooring.

3.1. Initial Conditions

For the proposed model, it is necessary to define the initial condition for all segments, as listed in Table 1.

Table 1. Initial conditions for proposed model.

Initial Conditions		
$\theta_1 = \frac{\pi}{4}$	$\theta_2 = 0$	$\theta_3 = \frac{\pi}{2}$
$\dot{\theta}_1 = 0$	$\dot{\theta}_2 = 0$	$\dot{\theta}_3 = 0$

All angle values in Table 1 are in radian. The initial angles are set for every segment to represent an untensioned mooring line. This method can be applied to a general mooring system as well. The parameters for the turbine, buoy, and mooring line are shown in Table 2; the turbine diameter was set to be the same as that of the SIMEC Atlantis Energy tidal turbine AR2000 [26] and the weight was half of its weight. The definitions of l_1, l_2 and l_3 are shown in Figure 2.

Table 2. The parameters of the turbine, buoy and mooring line.

System Parameters			
m_{buoy}	5 t	rotor rotation speed	1.25 rad/s
m_{turbine}	80 t	airfoil profile	NRELs814 [27]
l_1	30 m	number of blade	3
l_2	15 m	mooring line segment length	0.5 m
l_3	3 m	mooring line material	Dyneema
buoy radius	3 m	number of blade element	20

3.2. Sea States

Table 3 lists the sea states investigated in the simulations to obtain the thrust and torque on the turbine. Steep and swell waves are investigated, comparing how wave excitation on the buoy affects the load on the turbine. The assumed hypothetical site for the generic turbine was chosen off the north east coast of the Orkney islands, Scotland. This site provided a flow speed of approximately 2.5 [m/s] and an average depth of 50 [m] [28].

Table 3. Sea states.

Sea States	1	2	3	Harsh Winter
H_s [m]	2.665	1.07	1.008	10.12
T_z [s]	6.135	11.07	4.653	10.06
water depth [m]	50	50	50	50
steepness (H/gT)	0.0719	0.0099	0.0237	0.1027
wave model	3rd-order	linear	2nd-order	3rd-order

A 3 min window of 0.1 [s] time step was simulated for each sea states.

4. Results

Firstly, the results with and without wave excitation on the buoy are compared in the same sea states. In sea state 1, a three-step approximate wave–current interaction model was applied in this simulation because its steepness was larger than 0.02 [29]. However, the hub height dropped to approximately 22.5 [m] during the operation compared with the original height, which was set at 30 [m] from the seabed. Therefore, the hub height for the rigid supported turbine was set equal to that of the mooring supported one. Figure 7 exhibits the result in sea state 1. These results indicate that the mooring supported turbine can more effectively reduce the peak thrust on the turbine when compared with the rigid supported turbine. Furthermore, the results from considering wave excitation on the buoy indicate a different waveform without wave excitation. The mean values of the three curves are close: 1.019 [MN] for the rigid supported turbine, 1.019 [MN] for that without wave excitation on the buoy, and 1.016 [MN] for that with wave excitation on the buoy. However, the standard deviation of the thrust on the mooring supported turbine considering wave excitation on the buoy is 28.23 [kN] and that without wave excitation is 16.90 [kN], which are 69.69% and 41.73% of that on the rigid structure value of 40.50 [kN].

The results for torque indicate a different trend compared with that of the thrust. Torques on the mooring-supported turbine with and without wave excitation on the buoy both have more fluctuations than that of the rigid supported turbine. However, the mean values are similar, that is, 364.91 [kN·m], 364.66 [kN·m], and 361.98 [kN·m] for rigid, without, and with, wave excitation on the buoy, respectively. The respective standard deviations are 18.19 [kN·m], 87.14 [kN·m], and 83.41 [kN·m]. This is because of modifying the relative velocity in the vertical direction, which is discussed later in this section.

Figure 8 exhibits the result for the turbines operating in sea state 2. It shows a favorable performance in the reduction of peak loading both in thrust and torque and the wave excitation on the buoy provides a positive effect in load reduction. The reason is that the buoy will oscillate more regularly in the wave with long wave periods. In this sea state, the mean values of thrust are 1.260 [MN], 1.265 [MN] and 1.265 [MN] for rigid supported turbine, mooring turbine without and with wave excitation on a buoy, respectively. The standard deviations are 47.35 [kN], 11.59 [kN] (24.5% of 47.35 [kN]) and 6.56 [kN] (13.9% of 47.35 [kN]) separately. The average torque values are 694.47 [kN·m], 699.92 [kN·m] and 699.06 [kN·m] and the standard deviations are 58.19 [kN·m], 24.98 [kN·m] and 20.86 [kN·m].

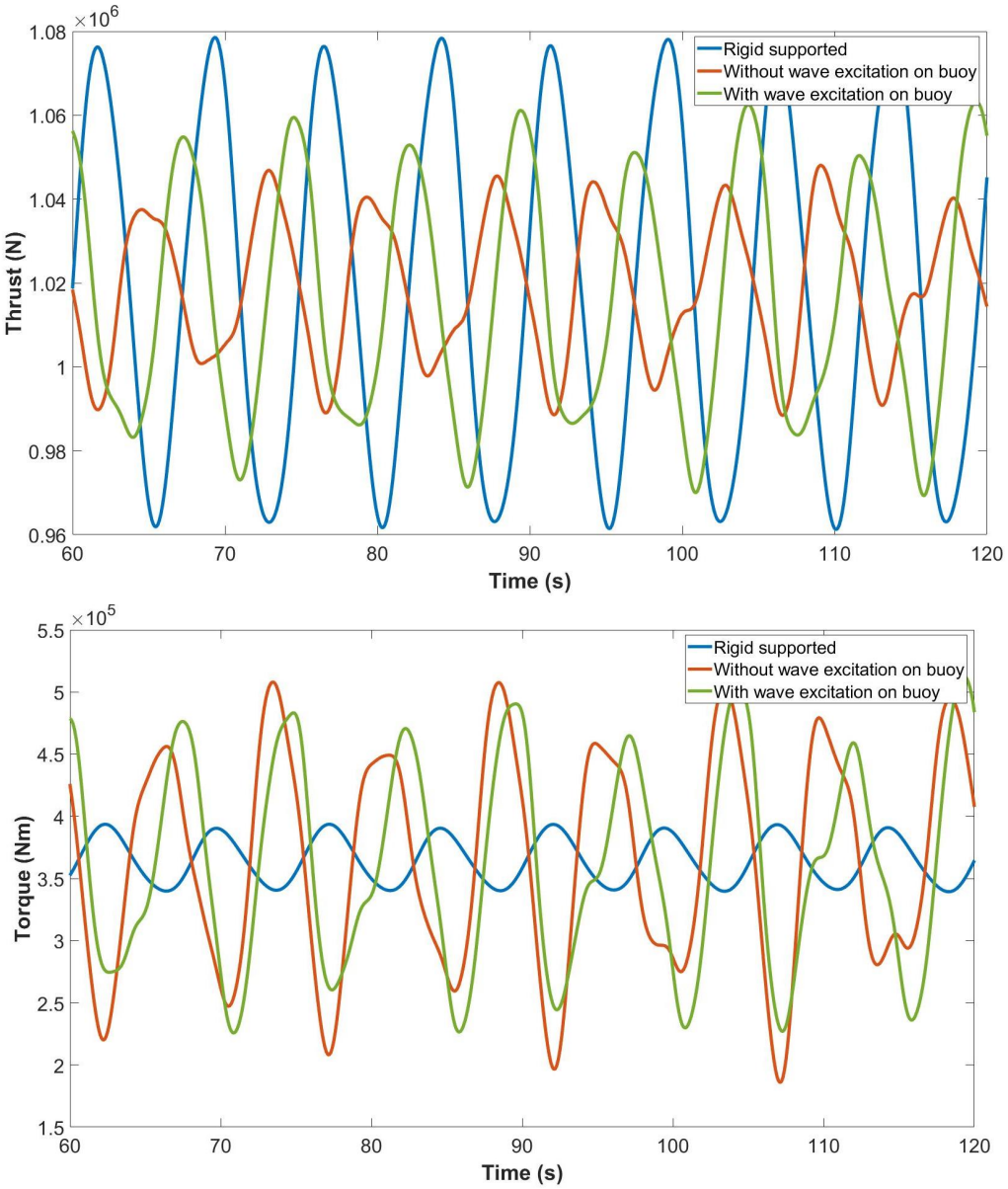

Figure 7. Thrust and torque in sea state 2.

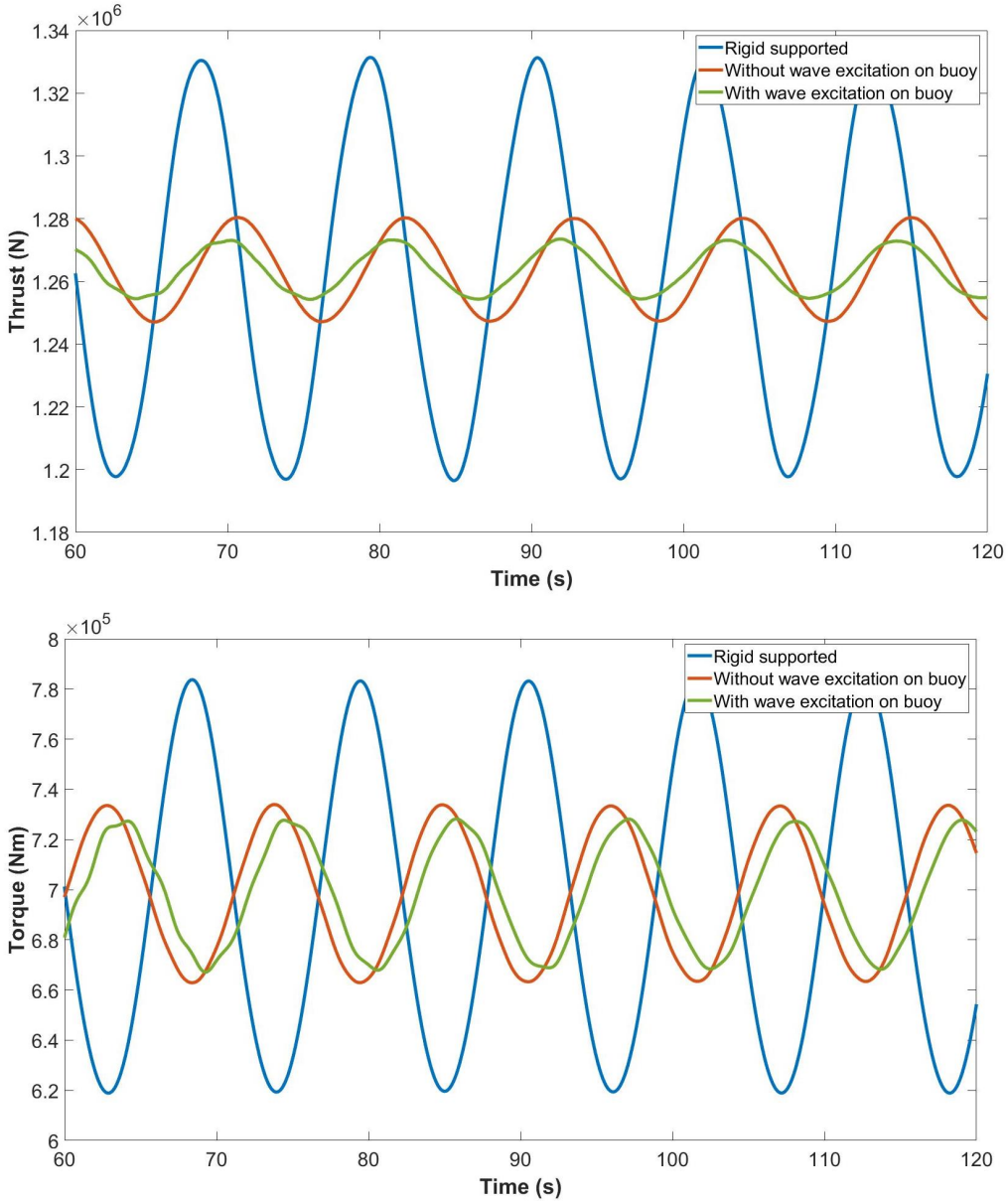

Figure 8. Thrust and torque in sea state 2.

In sea state 3, the performance of the system is different from all the sea states discussed so far as shown in Figure 9. The peak loading of thrust as a result of wave excitation on the buoy is larger when compared with the rigid supported turbine. The mean values of the thrust are 1.045 [MN], 1.044 [MN], and 1.040 [MN] for rigid supported turbine, mooring supported turbine without and with wave excitation on the buoy. The respective standard deviations are 5.82 [kN], 6.28 [kN] and 13.43 [kN]. The respective average torque values are 396.44 [kN·m], 394.84 [kN·m], and 390.25 [kN·m] and the standard deviations are 169.08 [kN·m], 20.73 [kN·m], and 35.48 [kN·m].

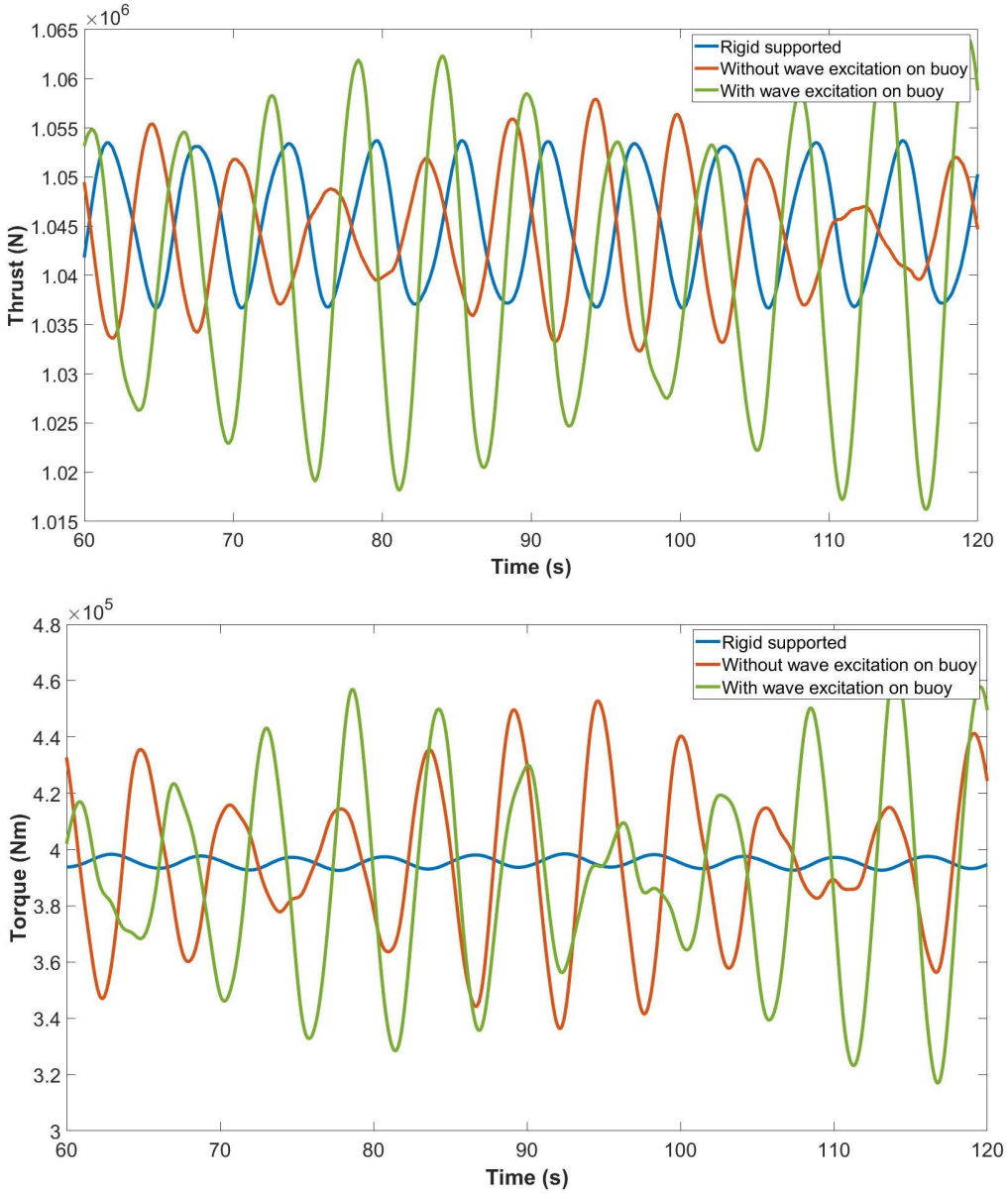

Figure 9. Thrust and torque in sea state 3.

The results for harsh winter conditions (the extreme storm sea state in the North Sea) are presented in Figure 10. The peak loading reduction in the thrust is similar to that in sea state 2. The mean values are 930.03 [kN], 897.42 [kN], and 894.36 [kN], respectively. The respective standard deviations are 390.80 [kN], 86.67 [kN] (22.2%), and 37.57 [kN] (9.6%). However, the torque has negative values, which indicate that the directions of the torque have reversed. In reality, this means that the turbine will be stalled due to displacement being significantly large enough for the velocities on blade elements to change (see Figure 11).

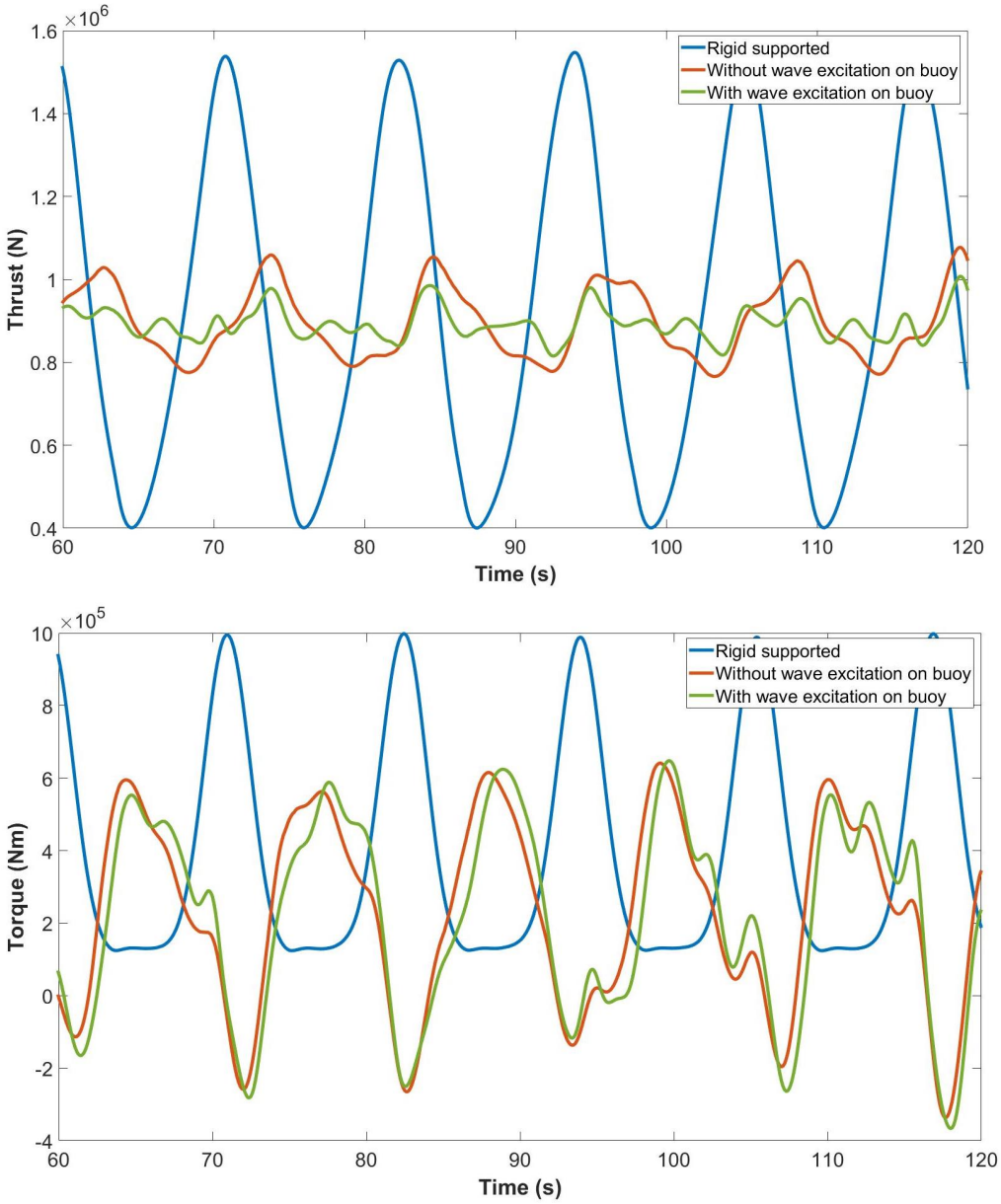

Figure 10. Thrust and torque in harsh winter.

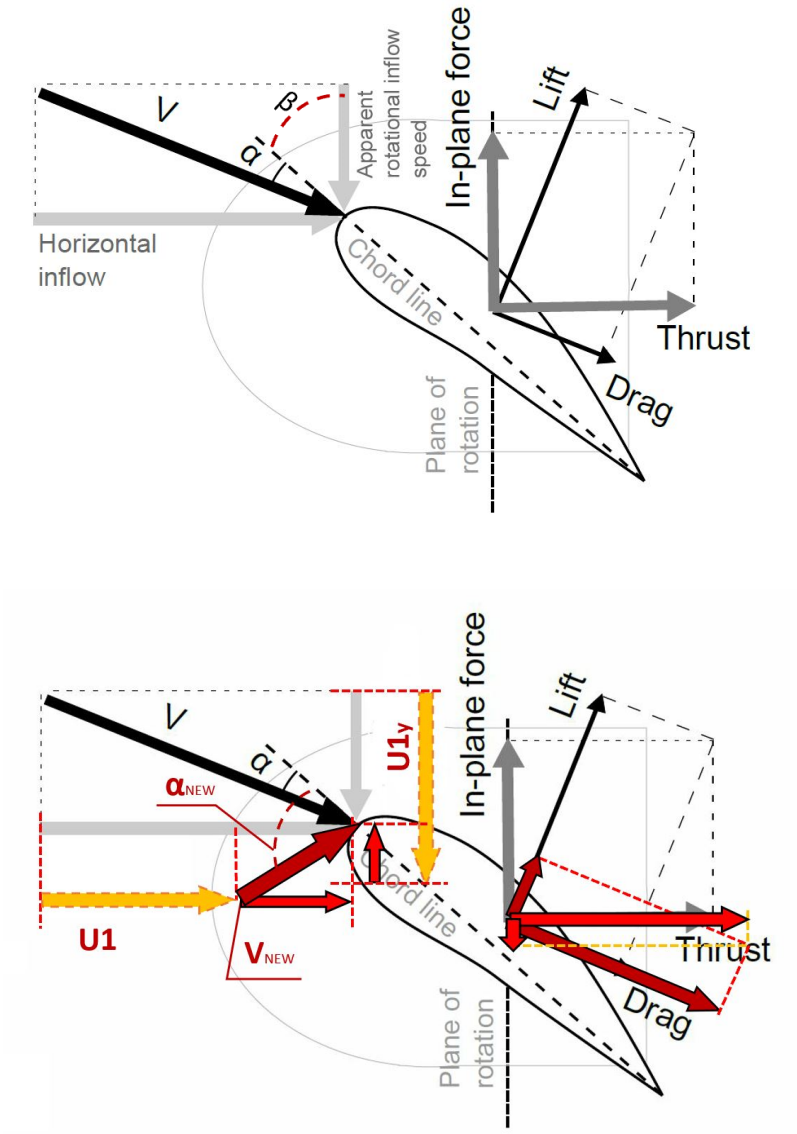

Figure 11. Inflow velocity vectors on blade sections in harsh winter.

5. Discussion

The thrust loading reduction in four listed sea states are favorable especially in the linear wave, but the reduction of torque on the rotor is not as satisfactory as the thrust; some findings are given in this section to discuss the noteworthy torque fluctuation.

5.1. Blade Section Velocities

In harsh winter sea states, the turbine moves heavily along the wave in the wave trough. The inertial velocity of the turbine, $\mathbf{U}_T$, is coupled with the wave–current velocity field and transferred to the local rotating blade coordinate system [24]. Two velocities, $U1$ and $U1y$, are obtained to modify the horizontal inflow and the apparent rotational inflow speed to calculate the relative velocity of the blade section. The new relative velocity results in a larger angle of attack, which generates a smaller lift force but a larger drag force on the blade section as shown in Figure 11. Therefore, the direction of the in-plane force is changed, which means the torque on the rotor has negative values and the blade is stalled. A blade profile that performs better than NRELs814 in larger angles of attack, or setting a pitch angle can be applied to avoid this phenomenon. However, this remains to be studied in the future.

5.2. Wavelength Factor

For sea state 3, the wavelength is 54.38 [m]. The water particle path reaches 27.19 [m] from the water surface, then it starts to decay dramatically. The turbine hub is at a height of approximately 21 [m] from the seabed and the turbine diameter is 20 [m], the upper part of the rotor is in the range of wave circular orbits, the lower part of the rotor is at the location where the wave decays rapidly as shown in Figure 12. This indicates that the wave affected approximately half of the rotor swept area during operation, but excited the buoy significantly. Furthermore, the load reduction for the mooring supported turbine does no better than that of the rigid supported turbine because the wave just reaches the hub of the turbine and affects half of the turbine; moreover, the superposition of the buoy and turbine oscillations in this sea state makes the performance unexpected. Further investigation of this kind of sea state will be part of future work.

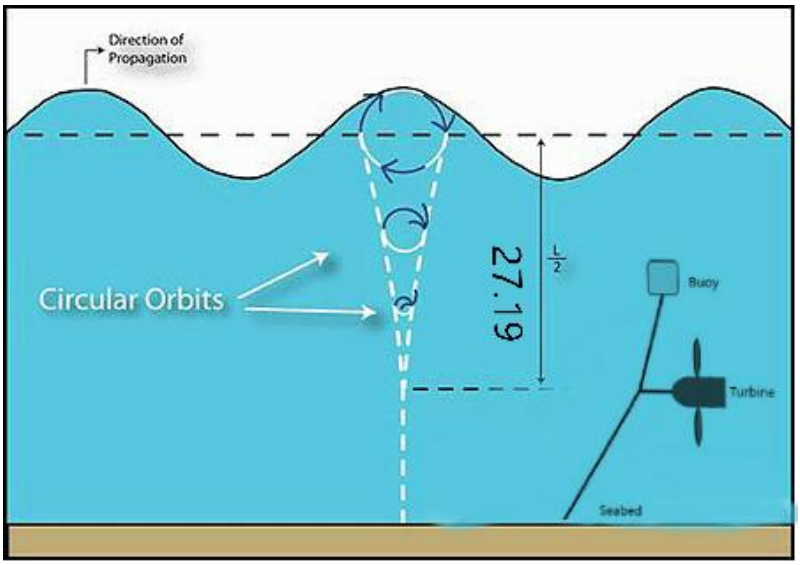

Figure 12. Water particle paths under waves in deep water and the turbine position.

5.3. Morison Effects

According to the results above, the variation of torque values on tension mooring supported turbines is larger than that of rigid supported ones in similar sea states. The reason for this is the added mass effects on blade sections and the inertia force added into the in-plane force to calculate the torque. The relative velocity term for a rigid supported turbine is only the wave particle velocity in the vertical direction transferred to the local rotating blade coordinate system. However, the inertia velocity of the turbine itself is coupled with the wave particle velocity in calculating the inertia force for the mooring supported turbine as in Equation (23); this results in an increase of inertia forces on blade sections in the mooring supported turbine. Then the total torque increases as the in-plane forces rise. Moreover, the method calculating the inertia force on the blade section for a rigid supported turbine may not be applicable for a turbine that can move in the water as a tension mooring supported turbine does.

Figure 13 presents the torque on the mooring supported turbine without Morison effects in sea state 1, and the torque reduces as expected. This indicates that the Morison effect, the added mass on the blade, plays a significant role in torque on a turbine that can move vertically. Moreover, the Morison effect module in BEMT could be improved in the future and the added mass effects on the mooring supported turbine blade should be further investigated.

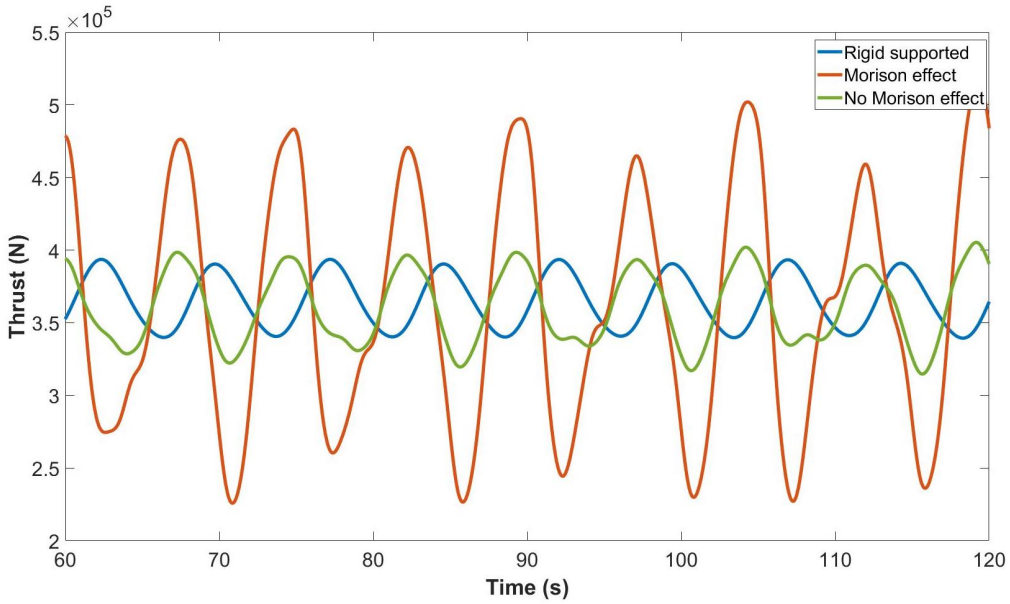

Figure 13. Morison effect in torque

6. Conclusions

The modified BEMT code for a tensioned mooring turbine itself is a very efficient tool and provides a fast simulation process. A 3 min simulation of a 0.1 [s] time step for 20 elements per blade and 0.5 [m] mooring line element lengths on a personal computer with 4 i7 cores takes approximately 1 h. The output contains various data, for example, inflow conditions on blade elements and forces on each element. The status of the turbine can be checked at every time step, and a simple animation can be generated for motions of the turbine. This is an efficient methodology for a highly dynamic system, such as a tensioned mooring supported turbine and other taut mooring systems, for checking its performance under various environmental conditions.

The dynamic marine climate causes significant load fluctuations on TSTs. This study found that the tensioned mooring supported system has a positive effect on thrust load reduction in most sea states. The system performance is satisfactory in swell waves, which have a long wavelength. Both thrust and torque fluctuations decrease significantly. The tensioned mooring-supported TSTs are useful for the swell environment or Stokes waves with long wavelengths. Therefore, installing this system can improve fatigue performance when compared with rigid supported TSTs.

In extreme conditions, such as harsh winter storms, the tensioned mooring supported TSTs significantly reduce the thrust loading; however, the turbine should be shut down and protected from potential damage to the blade due to negative torque. Furthermore, this stall phenomenon can be investigated by improving the blade design and adding a high angle of attack pitch angle to the blade so that the turbine can work under extreme conditions with a favourable load reduction.

The loading on the turbine is always calculated by a quasi-static method in most floating tidal turbine simulations, but the station keeping system uses a quasi-dynamic analysis. This study tried to combine the turbine loading calculation and dynamics of the mooring system by a modified BEMT code. However, this model can be enhanced with the addition of the torque calculation due to the added mass effect on blade sections caused by the quasi-static method, which results in the torque fluctuations. Further investigation should be done into the mass effects added to the mooring supported turbine blade.

In Stokes waves with short wavelengths, such as sea state 3 in the previous sections, the tensioned mooring supported TST can operate at the position where the wave particle paths can reach the whole turbine. For this, the diameter of the turbine must not to be too large and the buoy must supply a larger buoyancy when compared with the thrust loading

on the turbine. The turbine can operate at an appropriate location in a water column. However, the load reduction in this condition is still not as satisfactory as under the other sea states; the performance is approaching that of the rigid supported turbine. Therefore, to obtain a satisfactory load reduction in thrust, the tensioned mooring supported system must be designed for application in environments where the water is not excessively deep.

The vertical velocity component of the wave motion had a large influence on the rotor out-of-plane bending moment of a turbine. Furthermore, the tension mooring supported turbine itself has a vertical velocity because it can move in a vertical direction, thus the out-of-plane bending moment may be greater than a rigid supported turbine. Furthermore, the torque on the rotor is also affected by the vertical velocity of the turbine itself due to the Morison effect. It is obvious that the vertical motion of the turbine has a significant impact on the design of the TST's drive train or internal components; therefore, investigations of the influence of the turbine's vertical velocity on the rotor out-of-plane bending moment should be further investigated in the future. On the other hand, future modifications to the original Morison effects may not be applicable to the blade elements on a turbine that can move in a vertical direction; therefore, modifications of Morison effects should be improved in the future. In extreme sea states, such as harsh winter storms, greater blade profiles and pitch angles should be investigated in order to avoid the negative torque. Adjustable rotor speed will be an another research target in the future and should be applied to the model in order to produce a reliable torque result.

Author Contributions: Conceptualization, S.F. and C.J.; methodology, S.F.; software, S.F.; validation, S.F. and C.J.; formal analysis, S.F.; investigation, S.F.; resources, S.F.; data curation, S.F.; writing—original draft preparation, S.F.; writing—review and editing, S.F. and C.J.; supervision, C.J.; project administration, C.J.; funding acquisition, C.J. All authors have read and agreed to the published version of the manuscript.

Funding: This research was funded by EPSRC, UKRI grant No. EP/K013319/1.

Institutional Review Board Statement: Not applicable.

Informed Consent Statement: Not applicable.

Data Availability Statement: Data sharing not applicable No new data were created or analyzed in this study. Data sharing is not applicable to this article.

Acknowledgments: The authors would like to thank EPSRC, UK RI for their support of this research via the award of Grant No. EP/K013319/1 Reducing the Costs of Marine Renewables via Advanced Structural Materials (ReC-ASM).

Conflicts of Interest: The authors declare no conflict of interest.

References

1. Johnstone, C.; Pratt, D.; Clarke, J.; Grant, A. A techno-economic analysis of tidal energy technology. *Renew. Energy* **2013**, *49*, 101–106. [CrossRef]
2. Simecatlantis. Projects. Available online: https://simecatlantis.com/projects/meygen/ (accessed on 13 June 2019).
3. Emec Tidal Devices. Available online: http://www.emec.org.uk/marine-energy/tidal-devices/ (accessed on 30 September 2016).
4. Clarke, Joseph Andrew and Connor, Gary and Grant, Andrew and Johnstone, Cameron and Ordonez Sanchez, Stephanie. Contra-rotating marine current turbines: Single point tethered floating system—Stabilty and performance. In Proceedings of the 8rd European Wave and Tidal Energy Conference, Uppsala, Sweden, 7–10 September 2009.
5. Huang, S. Dynamic analysis of three-dimensional marine cables. *Ocean Eng.* **1994**, *21*, 587–605. [CrossRef]
6. Johanning, L.; Smith, G.H. Mooring design approach for Wave Energy Converter. *J. Eng. Marit. Environ.* **2006**, *220*, 159–174. [CrossRef]
7. Smith, J.L. Station keeping study for wec devices including compliant chain, compliant hybrid and taut arrangement. In Proceedings of the 27th Offshore and Arctic Marine Engineering Symposium, Estoril, Portugal, 15–20 June 2008.
8. Xu, S.; Wang, S.; Guedes Soares, C. Review of mooring design for floating wave energy converters. *Renew. Sustain. Energy Rev.* **2019**, *111*, 595–621. [CrossRef]
9. Coiro, D.P.; Troise, G.; Bizzarrini, N. Experiences in Developing Tidal Current and Wave Energy Devices for Mediterranean Sea. *Front. Energy Res.* **2018**, *6*, 136. [CrossRef]
10. Martynyuk, A.A.; Nikitina, N.V. The Theory of Motion of a Double Mathematical Pendulum. *Int. Appl. Mech.* **2000**, *36*, 1252–1258. [CrossRef]

11. Nevalainen, T.; Johnstone, C.; Grant, A. An Unsteady Blade Element Momentum Theory for Tidal Stream Turbines. In Proceedings of the 11th European Wave and Tidal Energy Conference, Plymouth, UK, 5–9 September 2015.
12. Maria Przybylska, W.S. Non-integrability of flail triple pendulum. *Chaos Solitons Fractals* **2013**, *53*, 60–74. [CrossRef]
13. Nevalainen, T.; Johnstone, C.; Grant, A. A Sensitivity Analysis on Tidal Stream Turbine Loads Caused by Operational, Geometric Design and Inflow Parameters. *Int. J. Mar. Energy* **2016**, *16*, 51–64. [CrossRef]
14. Elmas Anli, I.O. Classical and Fractional-Order Analysis of the Free and Forced Double Pendulum. *Engineering* **2010**, *2*, 935–949. [CrossRef]
15. Ohlhoff, A.P.R. Forces in the Double Pendulum. *ZAMM J. Appl. Math. Mech./Z. Angew. Math. Mech.* **2000**, *80*, 517–534. [CrossRef]
16. Wu, G.; Witz, J.; Ma, Q.; Brown, D. Analysis of wave induced drift forces acting on a submerged sphere in finite water depth. *Appl. Ocean Res.* **1994**, *16*, 353–361. [CrossRef]
17. Bossanyi, E. *BLADED for Windows Theory Manual*; Garrad Hassan and Partners Limited: Bristol, UK, 1997.
18. Gaonkar, G.; Peters, D. Review of dynamic inflow modeling for rotorcraft flight dynamics. In Proceedings of the 27th Structures, Structural Dynamics and Materials Conference, Structures, Structural Dynamics, and Materials and Co-Located Conferences, San Antonio, TX, USA, 19–21 May 1986. [CrossRef]
19. Schepers, J.G.; Snel, H. *Final Results of the EU JOULE Projects Dynamic Inflow*; Technical Report; US Government Printing Office: Washington, DC, USA, 1926.
20. Tuckerman, L.B. *Inertia Factors of Ellipsoids for Use in Airship Design*; Technical Report; US Government Printing Office, 1926.
21. Buckland, H.; Masters, I.; Chapman, J.; Orme, J. Blade Element Momentum Theory in Modelling Tidal Stream Turbines. In Proceedings of the 18th UK Conference on Computational Mechanics, Southampton, UK, 8–10 April 2010.
22. Chapman, J.C. Tidal Energy Device Hydrodynamics in Non-uniform Transient Flows. Ph.D. Thesis, Swansea University, Swansea, UK, 2008.
23. Whelan, J.M.R.; Graham, J.P. Inertia Effects on Horizontal Axis Tidal-Stream Turbines. In Proceedings of the 9th European Wave and Tidal Energy Conference, Lincoln, NE, USA, 24–26 June 2009.
24. Nevalainen, T. The Effect of Unsteady Sea Conditions on Tidal Stream Turbine Loads and Durability. Ph.D. Thesis, University of Strathclyde, Glasgow, UK, 2016.
25. British Oceanographic Data Centre. Wave Data. Available online: https://www.bodc.ac.uk/data/online_delivery/waves/search/ (accessed on 30 September 2016).
26. Simecatlantis. Simec Atlantis Energy Unveils World'S Largest Single Rotor Tidal Turbine, The AR2000. Available online: https://simecatlantis.com/2018/09/13/simec-atlantis-energy-unveils-worlds-largest-single-rotor-tidal-turbine-the-ar2000/ (accessed on 13 June 2016).
27. Airfoil Tool. NREL's S814 Airfoil (s814-nr). Available online: http://airfoiltools.com/airfoil/details?airfoil=s814-nr (accessed on 9 October 2021).
28. ABP Marine Environmental Research Ltd. Atlas of UK Marine Renewable Energy. Available online: https://www.renewables-atlas.info/ (accessed on 15 August 2017).
29. Fenton, J.D. A fifth-order Stokes theory for steady waves. *J. Waterw. Port Coastal Ocean Eng.* **1985**, *111*, 216–234. [CrossRef]